A brief analysis of ZTEM data from the Forrestania test site, WA

Daniel Sattel*
EM Solutions, USA
dsattel@earthlink.net

Ken Witherly
Condor Consulting, Inc., USA
ken@condorconsult.com

Michael Becken
GFZ Potsdam, Germany
becken@gfz-potsdam.de

SUMMARY

ZTEM is a helicopter-borne AFMAG system that measures the magnetic-field response in the frequency range 25-600 Hz of naturally occurring currents in the subsurface. The resolution of this system is analyzed by forward modeling and inverting synthetic ZTEM data using a 2D algorithm for a range of conductivity scenarios.

ZTEM data acquired at the Forrestania test site are compared with overlapping VTEM data. Conductivity-depth sections derived from both data sets show broad agreement, but indicate better spatial resolution for the VTEM data. The response due to bedrock conductor IR2 is strong for the VTEM system and subtle on the ZTEM profiles, which appear to be dominated by responses to larger, elongated structures. Products derived from the ZTEM data, including apparent conductivity, phase and Karous-Hjelt filtered grids appear to map geologic structure, complementing the information gathered from the VTEM data.

Key words: AFMAG, airborne electromagnetics, EM data modeling, inversion, natural-field EM.

INTRODUCTION

The ZTEM system was developed by Geotech Ltd to measure the AFMAG responses of naturally occurring subsurface currents, induced by far-away lightning discharges (Legault et al., 2009). The vertical component is measured from a moving helicopter platform, while the horizontal components are recorded on the ground at a base station. By comparison, the VTEM system measures the magnetic-field response due to currents induced in the subsurface by the transmitter the system is carrying (Witherly and Irvine, 2007).

Geotech has flown the VTEM and ZTEM system across two bedrock conductors at Forrestania, W.A., located approximately 350 km east of Perth. The overlap of data from both surveys allow for a direct comparison of the spatial resolution and depth penetration of the two systems. Before analysing the survey data, synthetic modelling of the ZTEM data is presented, to illustrate the strengths and limitations of that system.

SYNTHETIC ZTEM DATA

Synthetic ZTEM profiles were forward modeled and inverted using a 2D MT algorithm, developed by Constable and Wannamaker (deGroot-Hedlin and Constable, 1990; Wannamaker at al., 1987; deLugao and Wannamaker, 1996).

Synthetic modeling results are shown in Figures 1-3. A flying height of 80 m was modeled. Since the vertical magnetic field, due to plane-wave excitation (magnetotelluric Hz response) is zero above a 1D earth, the ZTEM system tipper-functions Tzx and Tzy, that are determined from the magnetic field observations by statistical analysis of the relationship

$$H_z = \begin{bmatrix} T_{zx} & T_{zy} \end{bmatrix} \begin{bmatrix} H_x \\ H_y \end{bmatrix} \quad (1)$$

show no response above a layered-earth. Hence, the ZTEM system is insensitive to one-dimensional or layered conductivity structures. In Equation (1), the vertical magnetic field is measured in the air, and the horizontal components are recorded with a fixed ground station. For the computation of synthetic across-strike profiles using a 2D modeling code, Equation (1) simplifies to

$$H_z = T_{zx} H_x \quad (2)$$

The sensitivity of ZTEM data to two-dimensional conductivity structures is demonstrated with the salt lake, regolith and tabular conductor models in Figures 1-3. The inversion fitted the data to a RMS error of 1.3, which has been determined as a representative target RMS for the modeling of survey data. Since these are synthetic data, the inversion would be able to achieve a better data fit, but this exercise is meant to demonstrate the resolution of actual ZTEM field data.

In Figure 1, the ZTEM system shows a strong Tzx response at the salt-lake edges and the 2D inversion resolves the conductivity of the salt lake very well, but doesn't indicate the presence of the regolith.

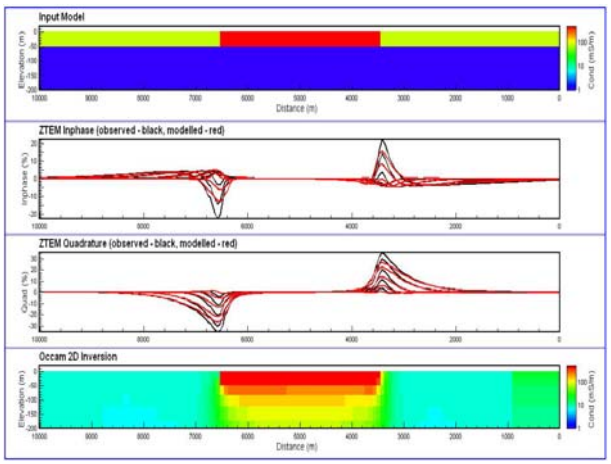

Figure 1. Observed and modelled ZTEM responses above a salt lake (50 m of 5 S/m), surrounded by regolith (50 m of 0.1 S/m) on a resistive half-space (0.0001 S/m).

Figure 2 shows that a regolith of laterally varying conductivity can show a moderate ZTEM response. The inversion recovers well the lateral conductivity gradient from the synthetic data. However, the modelled noise level does not allow for a good vertical resolution, which results in the blurred recovery of the true conductivity structure.

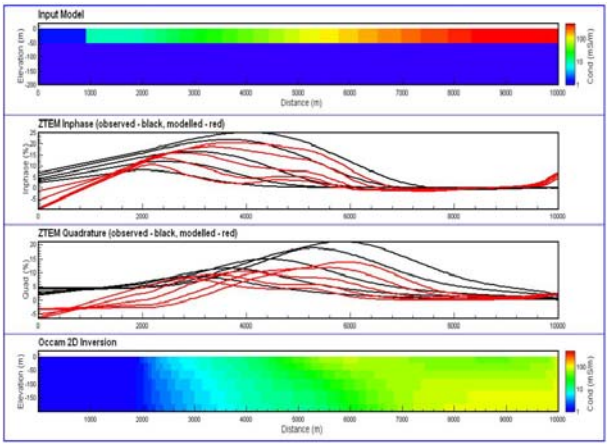

Figure 2. Observed and modelled ZTEM responses above regolith of laterally varying conductivity (50 m of 0.0015 – 0.1 S/m) on resistive half-space (0.001 S/m).

The ZTEM response across a tabular conductor under 100 m of overburden is shown in Figure 3. The ZTEM system shows a strong Tzx response above the conductor and the 2D inversion gives a good indication of the conductor's presence.

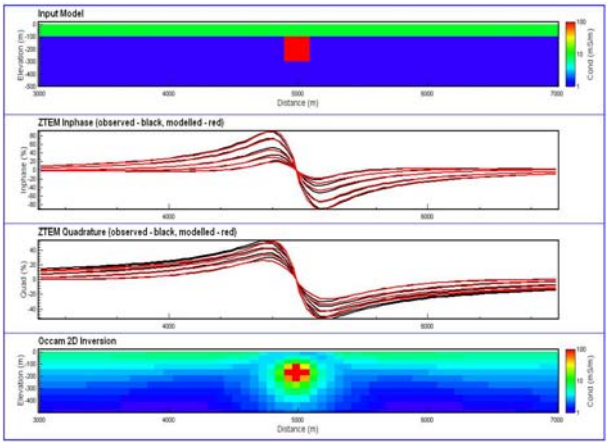

Figure 3. Observed and modelled ZTEM responses above prism (200 m x 200 m of 1 S/m) under overburden (100 m of 0.01 S/m) on resistive half-space (0.001 S/m).

FORRESTANIA SURVEY

The Forrestania EM test range is described on the website of Southern Geoscience Consultants (www.sgc.com.au). The ground covered by the VTEM and ZTEM surveys include two drilled, barren, semi-massive to massive sulphides (IR2 and IR4), hosted in highly resistive bedrock under a conductive overburden (10-20 S). Conductor IR2 is described as shallow (<100 m), highly conductive (>7,000 S), small (<75x75 m) and dipping 30-40 degrees to the north. It is well defined by surface, downhole and some airborne EM systems. The EM anomaly at the centre of VTEM profile 1075 (see Figure 4) clearly indicates the location of IR2. Conductor IR4 is described as deep (> 300 m), highly conductive (5,000-10,000 S), extensive in strike and plunge extent (> 500 m), limited in depth extent (100-150 m) and dipping 30-40 degrees to the north. Due to its depth, IR4 is difficult to detect with airborne EM systems. The VTEM profile of line 1160 shown in Figure 6 shows no indication for the presence of IR4.

The ZTEM survey was flown in late 2009 with a line spacing of 100 m. Survey lines were acquired north-south and east-west. Results from the north-south data set are included in the following discussion.

Modelling results from data across conductor IR2 are summarized in Figures 4 and 5. The conductivity-depth section shown in Figure 4 was derived from the VTEM data by layered-earth inversion. IR2 has been clearly mapped, albeit at greater depth than expected. The shown conductivity-structure was forward modelled to predict the expected ZTEM response using the 2D MT algorithm and taking into account the system elevation. The observed and predicted ZTEM data are shown in Figure 4, showing overall good agreement.

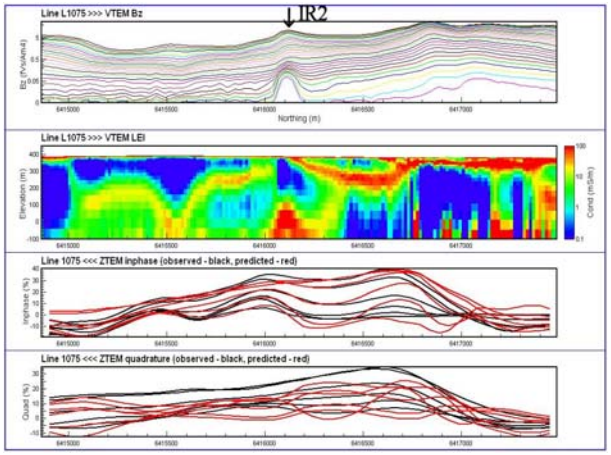

Figure 4. VTEM profile 1075 with derived conductivity-depth section (top), and observed and predicted ZTEM inphase and quadrature profiles (bottom). The ZTEM data were predicted from the VTEM-derived layered-earth section. The location of the bedrock conductor IR2 is indicated by an arrow.

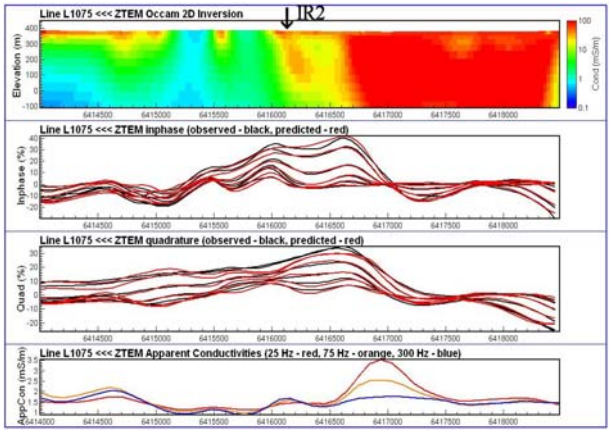

Figure 5. Line 1075, observed and modelled ZTEM responses with derived conductivity-depth section and apparent conductivity profile. The location of the conductor IR2 is indicated by an arrow.

Next, the ZTEM data were modelled using the 2D inversion algorithm by Constable and Wannamaker. The inversion result of the ZTEM data from Figure 4 is shown in Figure 5. The ZTEM-derived conductivity structure bears little resemblance with the VTEM-derived model. However, the conductor IR2 has been detected and modelled by the ZTEM data at the correct depth range and with the correct dip direction. Extensive conductive material is mapped at the northern end, consistently over most lines of this survey block. The discrepancy between conductivity-depth sections derived from VTEM and ZTEM data can be explained by ZTEM data being more sensitive to conductivity contrasts rather than elevated absolute conductivities, and current channelling being the major current excitation mode rather than induced vortex currents. The apparent conductivity profile shown in Figure 5, and explained below, shows a subtle peak at the location of IR2, which is overshadowed by a bigger and broader peak to the north, possibly corresponding to a shear zone.

VTEM and ZTEM profiles across IR4 with corresponding conductivity-depth sections are shown in Figure 6. Neither data set gives any indication for the presence of IR4. This is less surprising for the VTEM data, due to the depth of the conductor. It was hoped that, due the extensive strike length, the ZTEM data might be able to detect the conductor. As with the survey lines across IR2, the conductivity-depth sections derived from the two systems differ significantly, with the VTEM section indicating better spatial resolution.

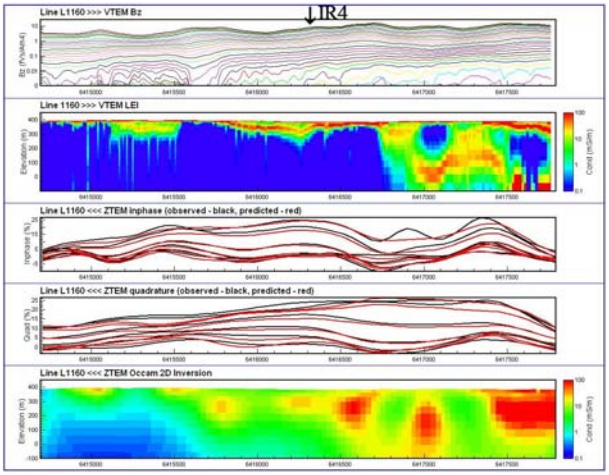

Figure 6: Line 1160, VTEM profile with derived conductivity-depth section (top) and ZTEM inphase and quadrature profiles with derived conductivity-depth section (bottom). The location of conductor IR4 is indicated by an arrow.

Conductivity-depth grids have been derived from the inversion results of all VTEM and ZTEM lines. Figure 7 shows the conductivity at different depths. Even though the two surveys had the same line spacing, the VTEM data provide superior spatial detail, especially at shallow depths. Extensive resistive material at intermediate depths was mapped by both systems in the southwestern quadrant. Conductive dentritic patterns mapped by the VTEM system agree well with similar patterns indicated by the ZTEM data, albeit at greater depth. There is good indication for conductor IR2 at shallow depths on the ZTEM-derived grids and at greater depths on the VTEM-derived grids.

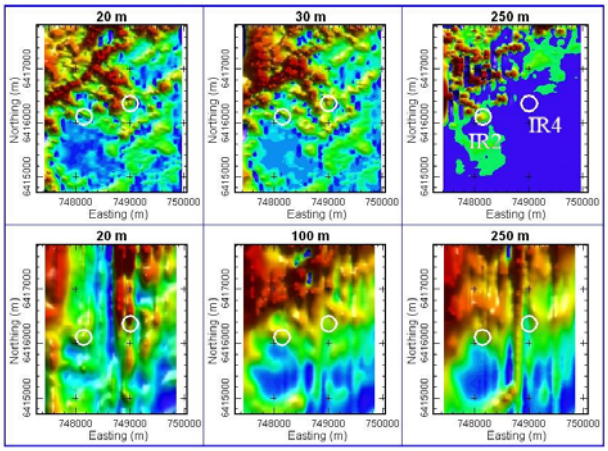

Figure 7: Top panel: conductivity-depth grids derived from VTEM inversions at depths 20 m, 30 m and 250 m. Bottom panel: conductivity-depth grids derived from ZTEM inversions at depths 20 m, 100 m and 250 m. The location of the known conductors is indicated by white circles, with IR2 being west of IR4.

Karous-Hjelt filter

Pseudo-sections derived with the Karous-Hjelt filter (Karous and Hjelt, 1983) can be useful to extract subtle conductors from the ZTEM profiles. The main property of the Karous-Hjelt filter is to turn cross-overs into peaks. Figure 8 shows pseudo-sections derived from the inphase profile of each frequency for line 1075. Even though the derivation of Karous-Hjelt sections is far less sophisticated than running 2D inversions, these sections agree overall with the 2D inversion result of Figure 5, mapping near-surface conductors, including IR2 and an extended pocket of conductive material to the east.

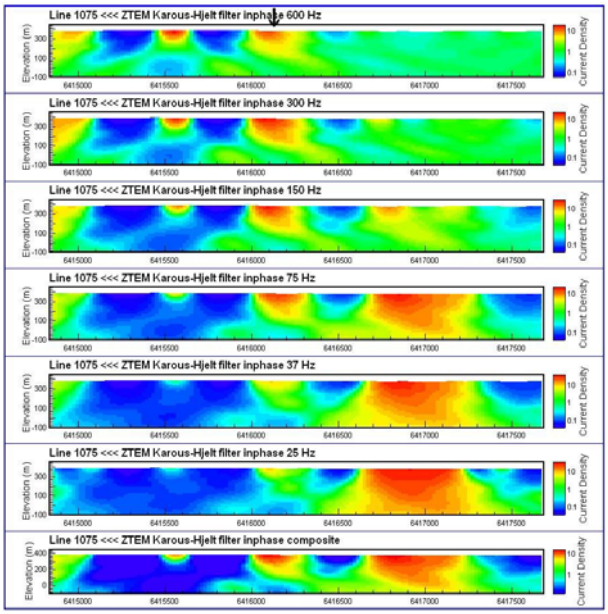

Figure 8: Line 1075, Karous-Hjelt sections derived from inphase ZTEM profiles with decreasing frequency from top to bottom and a composite section of all frequencies at the very bottom. The location of conductor IR2 is indicated by an arrow.

Near-surface grids of the Karous-Hjelt filtered ZTEM data are shown in Figure 9. These grids are similar to divergence grids generated by Geotech that are based on the VLF peaker derivation (Pedersen et al., 1994). The latter however makes use of the spatial derivatives of the Tzx and Tzy tippers, whereas the Karous-Hjelt-filtered grids shown were derived only from the Tzx data.

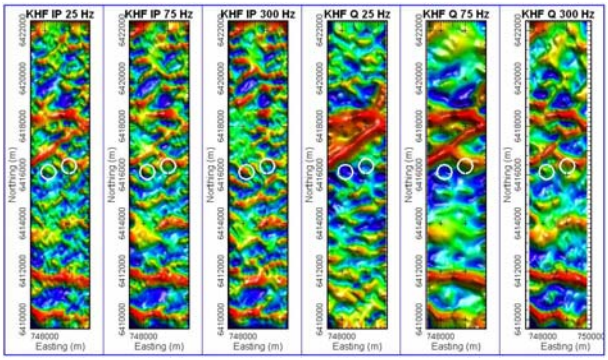

Figure 9: Karous-Hjelt near-surface grids, derived from the ZTEM inphase (left panels) and quadrature (right panels) responses. The location of the known conductors is indicated by white circles.

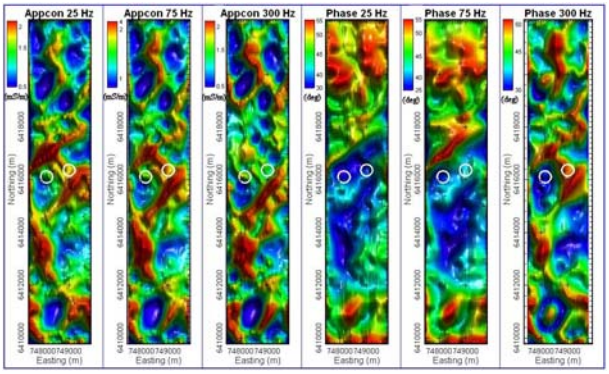

Figure 10: Apparent conductivities (left panels) and phases (right panels) derived jointly from ZTEM Tzx and Tzy responses 25-300 Hz. The location of the known conductors is indicated by white circles.

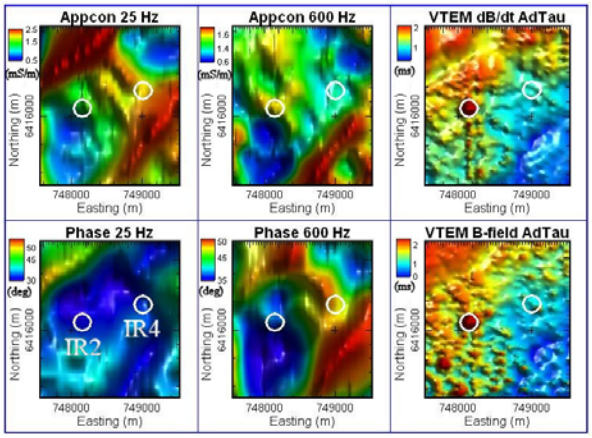

Figure 11: Close-up of some apparent conductivities and phases from Figure 9 and time-constants derived from VTEM dB/dt and B-field data. The location of the known conductors is indicated by white circles.

Apparent conductivity and phase

The derivation of apparent conductivity and phase from VLF data is discussed by Becken and Pedersen (2003). The method has been applied to the Forrestania ZTEM data, making joint use of the Tzx and Tzy tippers. The derived apparent conductivities and phases are shown in Figure 10. These images appear to indicate geological structures, such as SW-NE trending shears. A close-up of the area around the location of conductors IR2 and IR4 is shown in Figure 11. The apparent conductivities show elevated values at the location of IR2, especially for the higher ZTEM frequencies. The time-constants derived from the VTEM dB/dt and B-field data are also shown for comparison. There is strong indication for conductor IR2 on the time-constant images.

CONCLUSIONS

The analysis of VTEM and ZTEM data at Forrestania, WA, appears to indicate that the VTEM system offers better spatial resolution than ZTEM. In addition, the VTEM data show a strong response across a known sulphide body, whereas the corresponding ZTEM response is quite subtle. Some of the products derived from ZTEM data, including apparent conductivity grids, appear to map geological structure and, hence, complement the information gained from a VTEM survey.

ACKNOWLEDGMENTS

We are thankful to Geotech Airborne Pty Ltd for releasing the shown data for publication.

REFERENCES

Becken M., and Pedersen L.B., 2003, Transformation of VLF anomaly maps into apparent resistivity and phase: Geophysics 68, 497-505.

DeGroot-Hedlin, C. and S. Constable, 1990, Occam's inversion to generate smooth two-dimensional models from magnetotelluric data: Geophysics 55, 1613-1624.

De Lugao, P.P., and Wannamaker, P., 1996, Calculating the two-dimensional magnetotelluric Jacobian in finite elements using reciprocity, Geophys. J. Int., 127, 806-810.

Karous, M., and Hjelt, S.E., 1983, Linear filtering of VLF dip-angle measurements: Geophysical Prospecting 31, 782-794.

Legault, J.M., Kumar, H., Milicevic, B., and Hulbert, L., 2009, ZTEM airborne tipper AFMAG test survey over a magmatic copper-nickel target at Axis Lake in northern Sakatchewan: 79th International Exposition and Annual Meeting, SEG, Expanded Abstracts, 1272-1276.

Pedersen L.B., Qian, W., Dynesius, L., and Zhang P., 1994, An airborne tensor VLF system. From concept to realization: Geophysical Prospecting 42, 863-883.

Wannamaker, P.E., Stodt, J.A., and Rijo, L., 1987, A stable finite-element solution for two-dimensional magnetotelluric modeling: Geophysical Journal of the Royal Astronomical Society, 88, 277-296.

Witherly, K., and Irvine, R., 2007, Mapping targets of high conductance with the VTEM airborne EM system: 19th International Geophysical Conference and Exhibition, ASEG, Extended Abstracts.